

Prussian blue nanohybrid hydrogel combined with specific far-infrared based on graphene devices for promoting diabetic wound healing

Tingting Yu^{a,1}, Jiamin Zhang^{b,1}, Junwei Lai^{a,1}, Manjiao Deng^c, Ziyang Zhou^d, Zhanbin Xia^c, Caiying Zhong^b, Xinyue Feng^c, Yimin Hu^c, XuRan Guo^e, Wei Wei^e, Weichen Gao^e, Yi Zhang^{f,*}, Zhaobin Guo^{g,*}, Ke Hu^{b,*}

^a Department of Medical Genetics, School of Basic Medical Science, Nanjing Medical University, Nanjing 211166 Jiangsu, China

^b School of Biomedical Engineering and Informatics, Nanjing Medical University, Nanjing 210009 Jiangsu, China

^c Shenzhen Grahope Graphene Research Institute, Shenzhen 518063, China

^d College of Materials Science and Engineering, Donghua University, Shanghai 201620 China

^e Tianyuan Honor School, Nanjing Medical University, Nanjing 211166 Jiangsu, China

^f Department of Colorectal Surgery, The First Affiliated Hospital of Nanjing Medical University, Nanjing 210029 Jiangsu, China

^g Institute of Interdisciplinary Integrative Medicine Research, Shanghai University of Traditional Chinese Medicine, Shanghai 201203, China

ARTICLE INFO

Keywords:

Nanozymes
Graphene
Nanohybrid
Hydrogel
Energy medicine

ABSTRACT

Diabetic wounds are difficult to treat in nature due to their distinct pathophysiological characteristics, such as inflammation and/or oxidative stress, which offers an opportunity to employ nanozymes. However, nanozymes may cause safety concerns regarding the balance between enzymatic activity and cytotoxicity, as well as unclear metabolic pathways when used as free nanoparticles. To address this issue, we developed a Prussian blue nanohybrid hydrogel by pre-coupling of polymer materials and inorganic nanomaterials *via* covalent bond, improving the stability of the organic–inorganic interface as well as nanozymes within the nanohybrid hydrogel. The nanohybrid hydrogel retained the enzymatic activities of Prussian blue nanoparticles, and its enzymatic activities displayed temperature-dependent characteristics when in proximity to physiological temperature. In light of this, we combined graphene-based far-infrared photothermal therapy with nanohybrid hydrogel materials, in order to promote wound healing by thermal effects and improved enzymatic activity. Animal experiments demonstrated that this combination significantly accelerates diabetes wound healing, alleviating wound inflammatory responses, and promote collagen deposition and neovascularization. This innovative approach holds considerable promise for advancing the therapeutic potential of diabetic wound healing and offers new avenues for the development of next generation wound healing treatments.

1. Introduction

Diabetic wounds, due to their distinct pathophysiological characteristics and difficult-to-treat nature, have been extensively investigated [1]. The high blood glucose levels, microvascular damage, hypoxia, and abnormal inflammatory responses associated with diabetes lead to elevated levels of reactive oxygen species (ROS), which impair the activity of growth factors, disrupt cellular signaling, and hinder collagen synthesis and degradation [2]. Reducing ROS levels in the wound microenvironment has the potential to alleviate inflammation, promote collagen synthesis, and enhance the activity of growth factors, thereby

improving wound healing [3]. If successful, these approaches hold significant promise for advancing diabetic wound healing therapies.

Nanozymes, a distinctive class of nanomaterials, have garnered considerable attention due to their enzyme-like activities, which mimic the functions of natural enzymes [4,5]. Since their discovery, substantial research has focused on the biomedical applications of nanozymes, including *in vitro* diagnostics [6–8], drug delivery [9], photodynamic/photothermal therapy [10], and tissue engineering [11]. Particularly, their superior catalase-like and superoxide dismutase-like activities have demonstrated substantial potential for wound healing [12,13]. However, challenges remain regarding the balance between enzymatic

* Corresponding authors.

E-mail addresses: yizhang311@njmu.edu.cn (Y. Zhang), guozhaobin@shutcm.edu.cn (Z. Guo), kehu@njmu.edu.cn (K. Hu).

¹ The authors contribute equally to this work.

activity and cytotoxicity, as well as unclear metabolic pathways when used as free nanoparticle. To overcome these obstacles, researchers have increasingly explored the enhancement of nanozyme applications in wound healing through hybridization with other inorganic or organic materials, with composite hydrogel systems emerging as a prominent approach [14,15].

Hydrogels, characterized by their high water content and customizable functional groups within polymer networks, offer notable advantages in the development of composite materials [16,17]. Several strategies have been employed to combine nanozymes with hydrogels, including mechanical mixing, dispersion within the hydrogel network, and non-covalent interactions that form weak bonds with the hydrogel matrix [18]. Numerous studies have reported the development of composite materials using these methods, particularly for controlled drug [19] release and tissue repair [20]. However, these composite systems also exhibit limitations in wound healing applications. For example, the instability of organic–inorganic composite materials may lead to the release of nanomaterials into the circulatory system before they can achieve an ideal therapeutic effect [21]. Therefore, there is a need for more advanced strategies that combine nanozymes with hydrogels in a manner that integrates the advantages and functionalities of both materials while ensuring stability, thus providing valuable insights for designing novel wound-healing materials.

Nanohybrid materials, which consist of two or more distinct nanoscale components, leverage the unique properties of each constituent [22,23]. The nanoscale hybridization of these components often results in enhanced or entirely new properties, generating synergistic effects that improve the overall performance of the material [24]. Typically, nanohybrid materials are characterized by superior mechanical properties, stability, and biocompatibility compared to individual components or traditional composites [25]. Several reports have highlighted their application in diabetic wound healing, which mainly through regulating the interplay between oxidative stress and inflammatory responses [26–30]. Although nanohybrid materials have found applications in biomedicine, their integration with hydrogels remains relatively underexplored, with most studies focusing primarily on enhancing the mechanical properties of hydrogels. This limitation can be attributed to the inert nature of the inorganic nanomaterials previously used. By coupling nanozymes with commonly used hydrogel polymer monomers, it is possible to create nanohybrid units that maintain the adjustable mechanical properties of hydrogels while incorporating the catalytic activity of nanozymes. This approach satisfies the basic requirements for anti-inflammatory and wound-healing materials. Moreover, physical therapy techniques such as heat therapy, magnetic field treatment, and electrical stimulation are commonly employed in clinical settings to promote wound healing [31–33]. However, these therapies often fail to achieve synergistic effects when used in combination with conventional non-responsive wound healing materials. In contrast, some nanozymes are responsive to specific physical stimuli, with their therapeutic efficacy closely correlated to their enzymatic activity [34]. Therefore, integrating physical treatment methods with nanozyme-based hybrid hydrogels could potentially enhance wound healing, providing a novel paradigm for therapeutic interventions.

Building upon our previous research in nanozymes, biomimetic hydrogels, and non-invasive photothermal therapy [35–40], this study proposes a novel strategy for promoting diabetic wound healing through the use of Prussian blue nanohybrid hydrogels combined with far-infrared photothermal therapy. This approach offers several key advantages: (1) covalent coupling of Prussian blue nanozymes with gelatin methacrylate – previous studies on nanohybrid hydrogels have predominantly focused on combining polymer materials and inorganic nanomaterials during gelation, using chemical or physical methods to incorporate the nanomaterials into the hydrogel network via either covalent or non-covalent interactions. In contrast, the present study involves the pre-coupling of polymer materials and inorganic nanomaterials via covalent bonds, which are then employed as

crosslinkers to construct the nanohybrid hydrogel. This methodology enhances the stability of the organic–inorganic interface, improves crosslinking efficiency, and increases the stability of the nanozymes within the nanohybrid hydrogel. (2) Integration of far-infrared photothermal therapy with nanohybrid hydrogel – this strategy combines graphene-based far-infrared photothermal therapy with the nanohybrid hydrogel materials. Far-infrared radiation promotes wound healing through thermal effects, thereby enhancing the enzymatic activity of the nanozymes and improving the wound-healing efficacy of the nanohybrid hydrogel. Taken together, this novel strategy may offer a new paradigm for the treatment of chronic diabetic wounds.

2. Experimental section

2.1. Preparation and enzyme activity testing of Prussian blue nanohybrid units (PB@GelMA)

Prussian blue nanoparticles (PB NPs) were provided by Nanjing Dongna Biotechnology Co., Ltd. The preparation method is as follows: $\text{FeCl}_3 \cdot 6\text{H}_2\text{O}$ (0.2703 g, 0.001 mol) and $\text{C}_6\text{H}_8\text{O}_7 \cdot \text{H}_2\text{O}$ (0.6307 g, 0.003 mol) were added to 20 mL deionized water to form solution A. $\text{K}_4[\text{Fe}(\text{CN})_6] \cdot 3\text{H}_2\text{O}$ (0.4224 g, 0.001 mol) was dissolved in 20 mL deionized water to form solution B. Prior to the reaction, 10 mL of solution A was added to a reaction flask containing 60 mL deionized water to prepare PB NPs with different sizes and crystallinity. While stirring vigorously at 60 °C, 10 mL of solution A and 20 mL of solution B were added simultaneously at a rate of 40 mL/h. After the double injection, the reaction mixture was stirred for 2 h to obtain the final product. To purify the product, 20 mL of PB NPs solution was placed in a dialysis bag (molecular weight cutoff = 200 kDa) and soaked in 5 L deionized water for 5 days, with the external deionized water replaced multiple times during dialysis. The as-prepared Prussian blue nanoparticles (PB NPs) were subjected to elemental analysis using inductively coupled plasma (ICP) technique to determine their iron content. Accordingly, all PB NPs concentrations in this study were uniformly expressed in terms of iron concentration to ensure the accuracy and comparability of experimental data.

Construction of PB@GelMA Nanohybrid Unit: 2 mL PB NPs (0.25 mg/mL), 0.001 g 1-ethyl-3-(3-dimethylaminopropyl) carbodiimide (EDC, 5.216×10^{-6} mol), and 8 mL deionized water were mixed under mechanical stirring (500 rpm) at 37 °C for 15 min. Afterward, 10 mL of 0.04 % GelMA solution was added, followed by magnetic stirring for 30 min. The mixture was dialyzed at 55 °C for purification (molecular weight cutoff = 200 kDa).

Catalase-like Activity Test: 200 μL of phosphate buffer (pH = 8.23) was prepared, to which 20 μL of PB@GelMA (15.6 $\mu\text{g}/\text{mL}$) and 30 μL H_2O_2 solution (10 M) were added. The change in dissolved oxygen was measured using an oxygen meter (Presens OXY-1.ST, NTH needle-type probe).

Superoxide Dismutase (SOD)-like Activity Test: The total SOD activity was determined using a commercial SOD assay kit (WST-8 method). The SOD assay buffer and WST-8/enzyme working solution were prepared according to the kit's instructions. Different concentrations of PB@GelMA (Fe concentration: 0.75 $\mu\text{g}/\text{mL}$, 1.5 $\mu\text{g}/\text{mL}$, 4 $\mu\text{g}/\text{mL}$, 10 $\mu\text{g}/\text{mL}$) were set up, with sample and blank control groups as per the kit protocol. After incubating at 37 °C for 30 min, the absorbance at 450 nm was measured using a microplate reader to calculate the inhibition percentage.

Peroxidase-like Activity Test: TMB was chosen as the substrate for the colorimetric reaction. PB@GelMA dispersion (15.6 mg/L), TMB (10 mg/mL), H_2O_2 (10 M), and HAc-NaAc buffer (pH = 4.0) were mixed in a 2:1:3:20 ratio. The absorbance at 650 nm was recorded using a microplate reader, with measurements taken every 10 s for a total of 20 readings. The experiment was repeated in triplicate at 25 °C, 37 °C, and 43 °C.

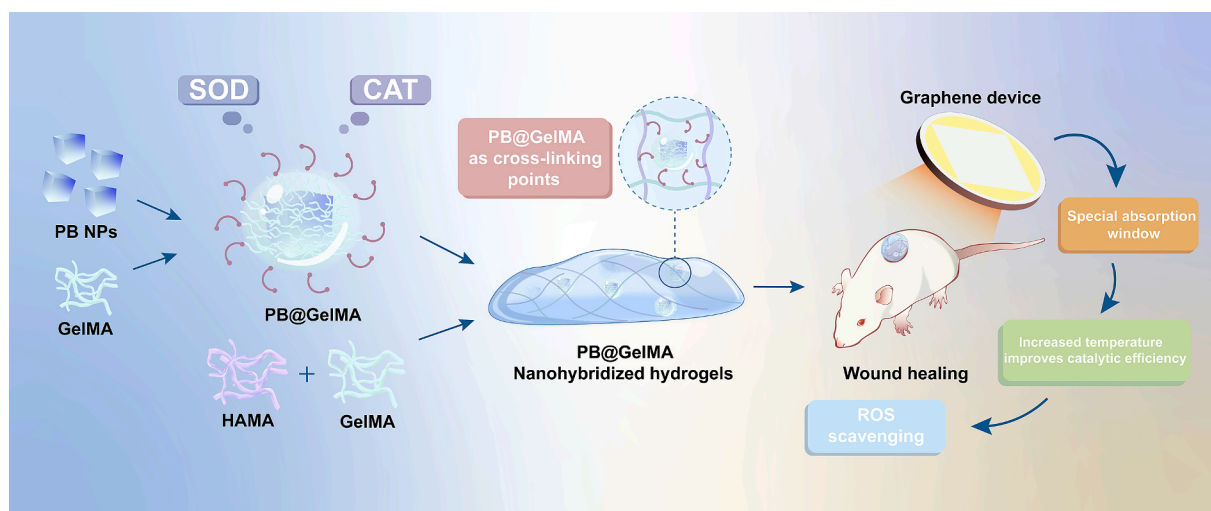


Fig. 1. Schematic illustration of the construction of nanohybrid hydrogels from Prussian Blue (PB) nanohybridization and their synergistic promotion of diabetic wound healing in conjunction with graphene-based devices through special far-infrared radiation. (For interpretation of the references to colour in this figure legend, the reader is referred to the web version of this article.)

2.2. Preparation of Prussian blue nanohybrid hydrogel

Gelatin methacrylate (GelMA, Jiangyin StamiBiotech Co., Ltd., Mw. 200 K, 8 % w/w), hyaluronic acid methacrylate (Shanghai Yujy Technology Co., Ltd., Mw. 150 k, 0.5 % w/w), and PB@GelMA (15 mg/L) were dispersed in deionized water. The nanohybrid hydrogel without PB@GelMA was used as the control, consisting of GelMA (8 % w/w) and hyaluronic acid methacrylate (0.5 % w/w) dispersed in deionized water. The mixture was stirred at 60 °C for 2 h until all components were completely dissolved and residual impurities were removed. Lithium phenyl-2,4,6-trimethylbenzoylphosphinate (LAP, Jiangyin StamiBiotech Co., Ltd., 0.5 % w/w) was added to the solution and sonicated until fully dissolved, followed by rapid filtration to remove impurities. The pre-polymer solution was injected into molds and subjected to photopolymerization (405 nm, intensity 500 mW/cm² for 5 min). Unless otherwise stated, all chemicals were purchased from Sigma-Aldrich.

2.3. Mechanical properties of Prussian blue nanohybrid hydrogels

The Young's modulus and stress relaxation of the hydrogels were characterized using a nanoindenter (Piuma, Optics11, Netherlands). The spherical optical probe of the nanoindenter had a tip radius of 47 μm and a stiffness of 0.35 N m⁻¹. During the Young's modulus measurement, the probe was set to indent 10 μm within 2 s, followed by a 1-second hold before unloading (mapping points: 25 points).

2.4. Enzyme activity tests of Prussian blue nanohybrid hydrogels

Catalase-like Activity of Nanohybrid Hydrogels: 30 μL of H₂O₂ (10 M) was mixed with 100 μL PBS buffer (pH = 8.23) at room temperature, then added dropwise onto pre-prepared nanohybrid hydrogel wells for imaging. **Peroxidase-like Activity of Nanohybrid Hydrogels:** TMB (10 mg/mL), H₂O₂ (30 %), and HAc-NaAc buffer (pH 4.0) were mixed in a 1:2:10 ratio, then added dropwise onto pre-prepared nanohybrid hydrogel wells for imaging.

2.5. Cell culture, in vitro antioxidant test, and live/dead staining

Raw 264.7 mouse macrophage leukemia cells were purchased from ATCC. Hydrogels in 24-well plates were sterilized, and 1 mL of α-MEM complete culture medium (with 10 % FBS) was added to each well for pre-culture at 37 °C and 5 % CO₂ for 24 h. The medium was then removed, and Raw 264.7 cells were seeded at a density of 40,000 cells

per well. After 5 days of culture, the cells were stimulated with 400 μM H₂O₂ for 4 h, followed by PBS washing (3 times). Live/dead cell staining was performed according to the manufacturer's instructions, and live (green) and dead (red) cells were observed under an inverted fluorescence microscope.

2.6. Infrared emission characteristics of graphene devices

Graphene devices were provided by Grahope New Materials Technologies Inc. The infrared emission spectrum was collected using a Fourier-transform infrared spectrometer (Thermo Fisher, Nicolet iS50). The light source was set to external, and the detector was a deuterated triglycine sulfate (DTGS) detector. The beam splitter used was KBr. Single-beam mode was selected, and the measurement range was 400–4000 cm⁻¹ with a resolution of 8 cm⁻¹, performing a total of 48 scans. The data were converted to wavelength to obtain the final spectrum. Infrared absorption spectra were also measured using the Fourier-transform infrared spectrometer (Thermo Fisher, Nicolet iS50). The external fiber probe with a germanium tip was coupled to the FTIR system using an attenuated total reflectance (ATR) configuration. The measurement range was 400–4000 cm⁻¹ with a resolution of 8 cm⁻¹, performing a total of 64 scans. The probe was placed in the air for background data collection, then applied to the surface of the test subject (mouse or human) and pressed for approximately 1 min to collect data. The resulting data were processed with advanced ATR correction.

2.7. Animal model, wound healing experiments, and related analysis

Sixty 8-week-old male SD rats (250–300 g) were injected with streptozotocin (40 mg/kg) dissolved in citrate buffer (pH = 4.5). Three weeks later, rats with blood glucose levels > 16.1 mmol/L on two consecutive measurements were defined as diabetic rats. The diabetic rats were anesthetized with 4 % pentobarbital sodium (30 mg/kg) via intraperitoneal injection, and hair was shaved from the back. A full-thickness wound of 10 mm diameter was created using a skin biopsy punch on both sides of the back. The wounds were treated with: 1) blank control, 2) graphene device only irradiation, 3) GelMA hydrogel, 4) PB@GelMA hydrogel, 5) PB@GelMA hydrogel + graphene irradiation. Groups 1 and 2 received physiological saline post-wounding, while groups 3, 4, and 5 received hydrogel treatment. Each group had 6 rats. Graphene device irradiation conditions: after stabilizing the device surface temperature at 100 °C, the rats were placed 15 cm from the graphene device surface and irradiated for 40 min twice daily. Wound

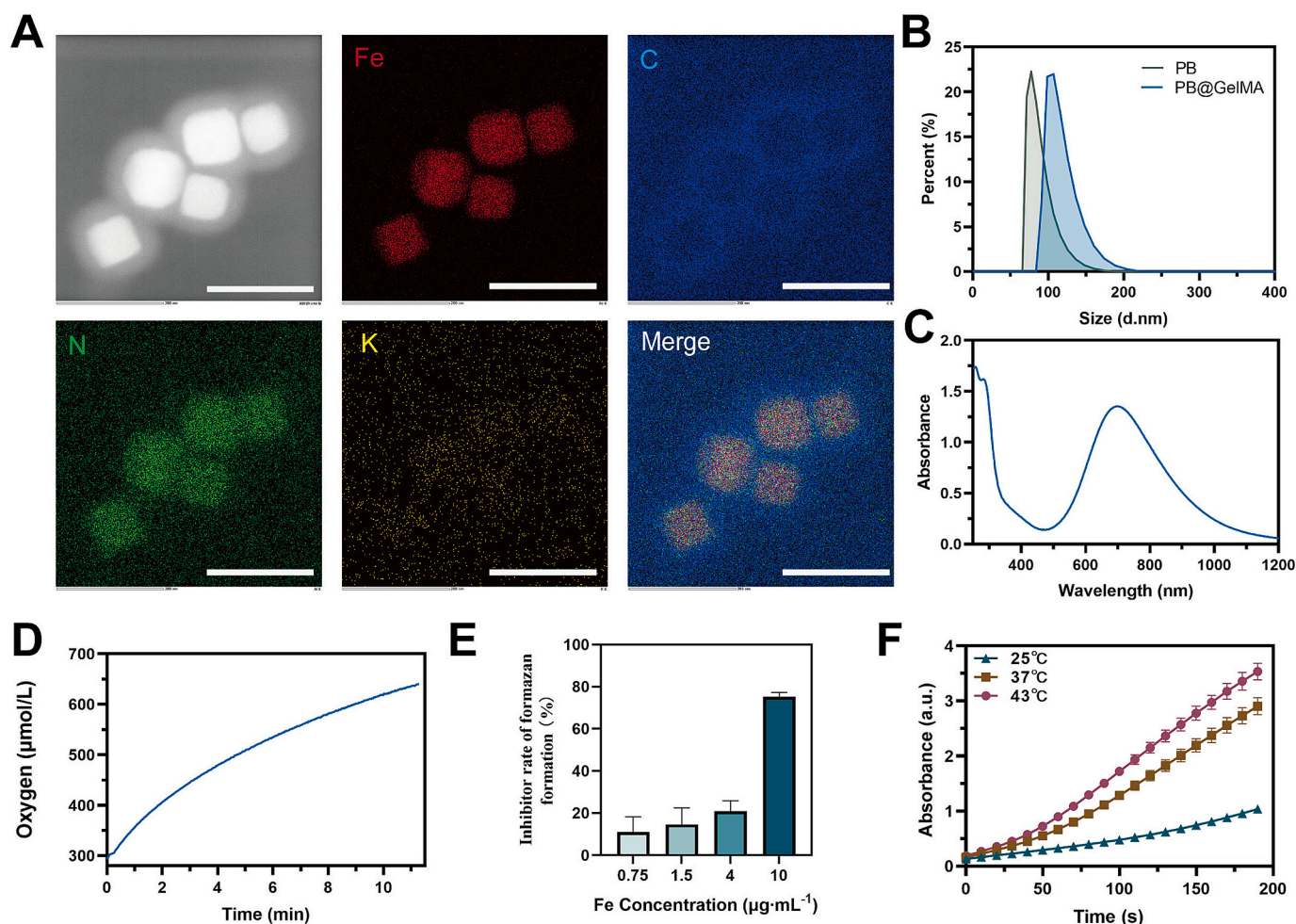


Fig. 2. Construction of PB@GelMA nanohybridization hydrogel: A) Scanning transmission electron microscopy (STEM) characterization of the PB@GelMA hybrids; B) Hydrodynamic size of the nanohybrid units; C) UV-Vis spectral characteristics; D) Peroxidase-like activity; E) Superoxide dismutase (SOD)-like activity; F) Peroxidase-like activity at different temperatures. Scale bars represent 200 nm.

images were taken on days 0, 6, and 9, and wound tissues were excised on days 6 and 9 for histological analysis. Hematoxylin and eosin (H&E) and Masson's trichrome staining were performed on day 6 and day 9. Immunofluorescence staining for CD86 and CD206, as well as immunohistochemistry for IL-10 and TNF- α , were conducted to evaluate the inflammatory response in the wounds. Immunohistochemistry for collagen was performed to assess collagen deposition in granulation tissue, and immunohistochemistry for CD31 and α -SMA was performed to analyze vascularization and smooth muscle cell activity. The animal experiment was approved by the Experimental Animal Welfare Ethics Committee of Nanjing Medical University (IACUC-2304002).

2.8. Statistical analysis

Statistical analysis was performed using GraphPad Prism (version 8.2.1). For all experiments with error bars, the standard deviation (SD) is calculated, and the data are presented as mean \pm SD. Data represent the average of at least three independent experiments ($n = 3$) or representative data from independent experiments. Co-localization analysis was performed using ImageJ (Fiji-win64 version) and the "Color2" plugin to calculate the Pearson correlation coefficient (R value). $P < 0.05$ is considered as statistically significant.

3. Results

We have developed Prussian blue nanohybrid units (PB@GelMA)

based on Prussian blue nanoparticles (PBNPs) with clinical translation potential and methacrylated gelatin (GelMA). Building on this, we used the nanohybrid unit as a crosslinking site and co-polymerized it with methacrylated hyaluronic acid (HAMA) and GelMA to fabricate biomimetic nanohybrid hydrogels, which were subsequently applied to promote diabetic wound healing. Fig. 1 illustrates our design strategy. This biomimetic nanohybrid hydrogel effectively adapts to the mechanical environment of the wound tissue, while also performing catalase (CAT)-like and superoxide dismutase (SOD)-like activities by scavenging reactive oxygen species (ROS), thus promoting wound healing. Furthermore, we integrated the nanohybrid hydrogel with infrared non-invasive photothermal therapy based on a special graphene device, a concept we previously proposed. By elevating the wound temperature, this approach not only provides thermal therapy but also enhances the enzymatic activity of the nanohybrid hydrogel, achieving synergistic treatment to alleviate inflammation and promote tissue regeneration (Fig. 1).

3.1. Construction and characterization of PB@GelMA nanohybrid hydrogels

To characterize the structure and fundamental properties of the Prussian blue nanohybrid units, we performed imaging and elemental analysis using scanning transmission electron microscopy (STEM) (Fig. 2A). The results revealed that the Prussian blue nanoparticles exhibited well-formed crystallinity. Elemental analysis further showed a

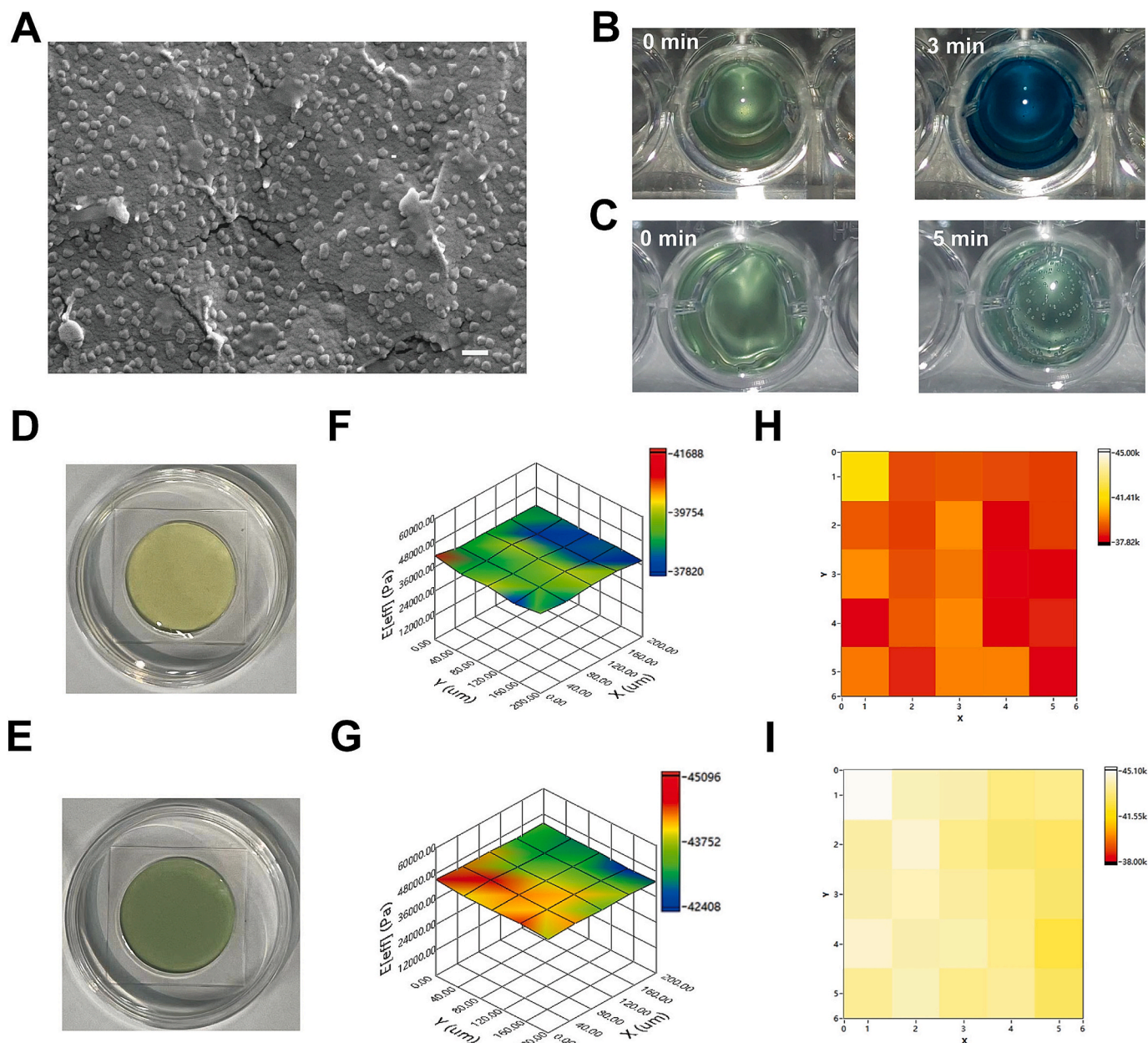


Fig. 3. Fabrication of PB@GelMA nanohybrid hydrogels: A) Scanning electron microscopy (SEM) images of the PB@GelMA nanohybrid hydrogels; B) Peroxidase-like activity of the nanohybrid hydrogels; C) Catalase-like activity of the nanohybrid hydrogels; D) and E) Photographs of GelMA hydrogel and PB@GelMA hydrogel; F) and G) Three-dimensional (3D) heat maps of Young's modulus mapping for GelMA hydrogel and PB@GelMA hydrogel; H) and I) Two-dimensional (2D) heat maps of Young's modulus mapping for the hydrogels. Scale bars represent 200 nm.

distinct carbon layer surrounding the core, indicating the successful coupling of GelMA with the citric acid on the surface of Prussian blue. Hydrodynamic size measurements indicated a significant increase in the size of the nanohybrid units compared to the original particles, while still maintaining excellent size uniformity (Fig. 2B). UV-Vis spectroscopy results demonstrated a clear absorption peak around 720 nm (Fig. 2C), consistent with the characteristic absorption of Prussian blue in the visible light range. The Prussian blue nanohybrid units exhibited strong catalase-like activity (Fig. 2D), superoxide dismutase-like activity (Fig. 2E), and peroxidase-like activity (Fig. 2F). Additionally, enzyme activity was significantly enhanced at elevated temperatures, providing a solid foundation for subsequent biological applications. This temperature elevation provides higher kinetic energy to molecules in the reaction system, effectively reducing the activation energy and significantly enhancing the catalytic reaction rate. This phenomenon is

consistent with the photothermal catalytic enhancement effects reported in numerous studies [41,42]. Considering the relationship between Prussian blue (PB) concentration and absorption characteristics, we systematically investigated the UV-Vis absorption spectral features by establishing three concentration gradients (Fig. S1). The experimental data indicate that the absorbance of characteristic absorption peaks exhibits a distinct concentration-dependent enhancement with increasing PB concentration, providing a reliable basis for quantitative analysis.

PB@GelMA retains the polymerization capability of GelMA as a hydrogel monomer. Scanning electron microscopy (SEM) images revealed that PB@GelMA nanoparticles were uniformly dispersed within the hydrogel, providing preliminary evidence that the nanoparticles serve as crosslinking points in the nanohybrid hydrogel (Fig. 3A, Fig. S2). Furthermore, the nanohybrid hydrogel maintained the

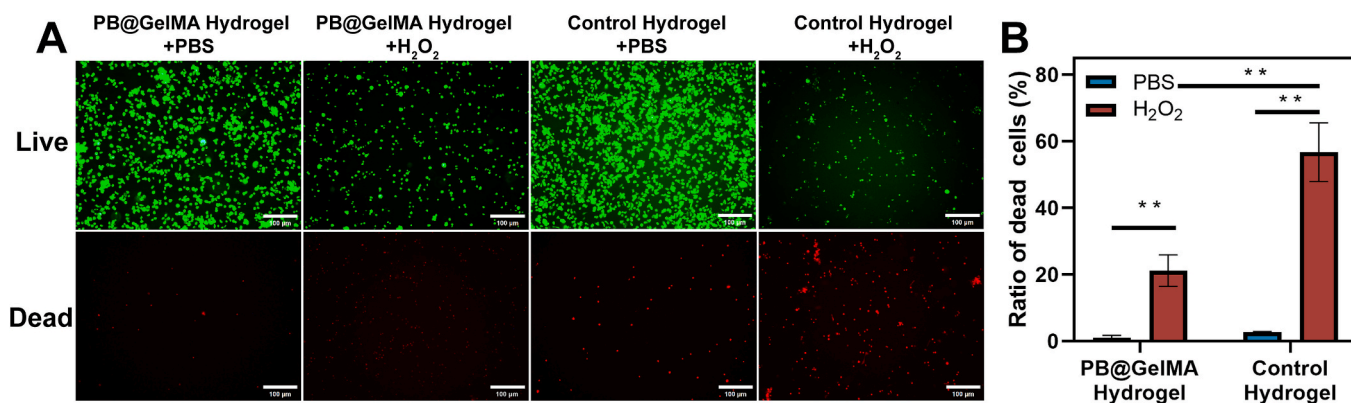


Fig. 4. In vitro antioxidant capacity characterization of PB@GelMA nanohybrid hydrogels: A) Live/dead cell staining images of PB@GelMA nanohybrid hydrogels; B) Quantitative statistical analysis of live/dead cell ratio. ** $p < 0.01$. Scale bars represent 100 μm .

peroxidase-like (Fig. 3B) and catalase-like (Fig. 3C, Supplementary Movie 1) activities of the Prussian blue nanoparticles. In comparison with pure polymer hydrogels prepared by co-polymerization of GelMA and HAMA (Fig. 3D, Supplementary Movie 2), the nanohybrid hydrogel made using PB@GelMA as the crosslinker and GelMA and HAMA as the monomers exhibited a distinct bluish-green appearance (Fig. 3E). These results confirm the stable presence of Prussian blue, which did not undergo significant changes in its physicochemical properties during crosslinking. 3D mechanical heatmaps showed that the Young's modulus of the Prussian blue nanohybrid hydrogel (Fig. 3F) was significantly higher than that of the pure polymer hydrogel (Fig. 3G). Additionally, 2D mechanical heatmaps indicated that the material were mechanically uniform, with properties closely resembling those of the wound tissue (Fig. 3H and I).

3.2. Biocompatibility of PB@GelMA nanohybrid hydrogels

We selected macrophage Raw 264.7 cells as the cell model to evaluate the biocompatibility and antioxidant capacity of the Prussian blue nanohybrid hydrogel. Raw264.7 cells were cultured on the surface of the hydrogel, and live/dead cell staining results number of cell deaths were observed on the surface of the pure polymer hydrogel, whereas significantly fewer cells died on the surface of the Prussian blue nanohybrid hydrogel (Fig. 4A). Quantitative analysis of the live/dead cell ratio confirmed this trend (Fig. 4B). These results indicate that the Prussian blue nanohybrid hydrogel possesses strong reactive oxygen species (ROS) scavenging capability, thereby protecting cells from ROS-induced damage. Prussian blue nanozymes (PBNs) synergistically scavenge ROS by mimicking the multi-enzyme activities of SOD, CAT, and POD. Their CAT-like activity decomposes H₂O₂ into water and oxygen, blocking the ROS cascade. By reducing ROS levels, PBNs alleviate oxidative stress and suppress the release of pro-inflammatory factors, while promoting macrophage polarization toward the anti-inflammatory M2 phenotype and enhancing the secretion of repair factors. This design accelerates diabetic wound healing through multi-enzyme synergistic antioxidant effects, regulation of the inflammatory microenvironment, and improvement of hypoxia, protecting cells from oxidative damage.

3.3. Synergistic promotion of diabetic wound healing by PB@GelMA nanohybrid hydrogels and graphene-based far-infrared emission devices

The results in Fig. 2 demonstrate that the enzymatic activity of the nanohybrid hydrogel increases with temperature. Based on these findings and our previous research on graphene-based non-invasive photothermal therapy [38,40], we hypothesize that the combination of this nanohybrid hydrogel with graphene photothermal therapy could have a synergistic therapeutic effect on wounds prone to bacterial infections, such as those in diabetic patients. To test this hypothesis, we developed a

chronic wound model in diabetic rats and evaluated the effect of Prussian blue nanohybrid hydrogel combined with non-invasive photothermal therapy on wound healing. The experimental timeline and appearance of the graphene device are presented in Fig. 5A and B, respectively. Raman spectroscopy of the device confirmed that the core material is graphene monolayer (Fig. 5C). The electromagnetic waves emitted by the device upon electrical stimulation did not exhibit significant changes in the infrared spectral peaks with temperature variations, and they matched the characteristic absorption window of infrared spectra for skin of both rats and humans (Fig. 5D, blue strip indicates the region). The device demonstrated excellent infrared emission stability and uniformity at different input powers (Fig. 5E, Figs. S3–S5). Additionally, the temperature of the rat wound site increased by approximately 3 °C after infrared irradiation, with the physiological status of the rats remaining normal before and after a single irradiation session (Fig. 5F).

To further compare the effects of Prussian blue hydrogel and graphene photothermal therapy on diabetic wounds, five experimental groups were established: Blank Control, Graphene Irradiation (GI) only, Control Hydrogel, PB@GelMA Hydrogel only, and PB@GelMA Hydrogel + Graphene Irradiation (PB@GelMA Hydrogel + GI). Wound area measurements indicated that, on both day 6 and day 9, the GI group and the PB@GelMA Hydrogel group exhibited similar results, both significantly smaller than the Blank Control and Control Hydrogel groups. The PB@GelMA Hydrogel + GI group showed the smallest wound area (Fig. 5G and H). These findings suggest that both Prussian blue nanohybrid hydrogel and graphene-generated far-infrared radiation individually promote wound healing, with the combined therapy showing the most significant healing effect. The results further validate our hypothesis that the far-infrared radiation generated by the graphene device not only promotes wound healing but also enhances the ability of the Prussian blue nanohybrid hydrogel to scavenge reactive oxygen species (ROS) at the wound site, thereby facilitating a synergistic anti-inflammatory effect and accelerating tissue regeneration.

Based on these findings, histological analysis of the wound tissue was conducted using hematoxylin-eosin (HE) staining and Masson's trichrome staining. The staining results were consistent with the observed wound area reduction. HE staining demonstrated that both the special far-infrared radiation generated by the graphene device and the Prussian blue nanohybrid hydrogel effectively reduced inflammation, with their combined treatment showing a more pronounced effect (Fig. 6A). Masson's trichrome staining revealed that collagen deposition in the graphene far-infrared group and the Prussian blue nanohybrid hydrogel group was greater than in the Blank Control and pure polymer hydrogel groups. Notably, the collagen deposition in the combined treatment group was significantly higher than that in all other groups (Fig. 6B).

We further performed immunofluorescence staining of pro-inflammatory (M1-type) macrophage marker CD86 (Fig. 7A) and pro-

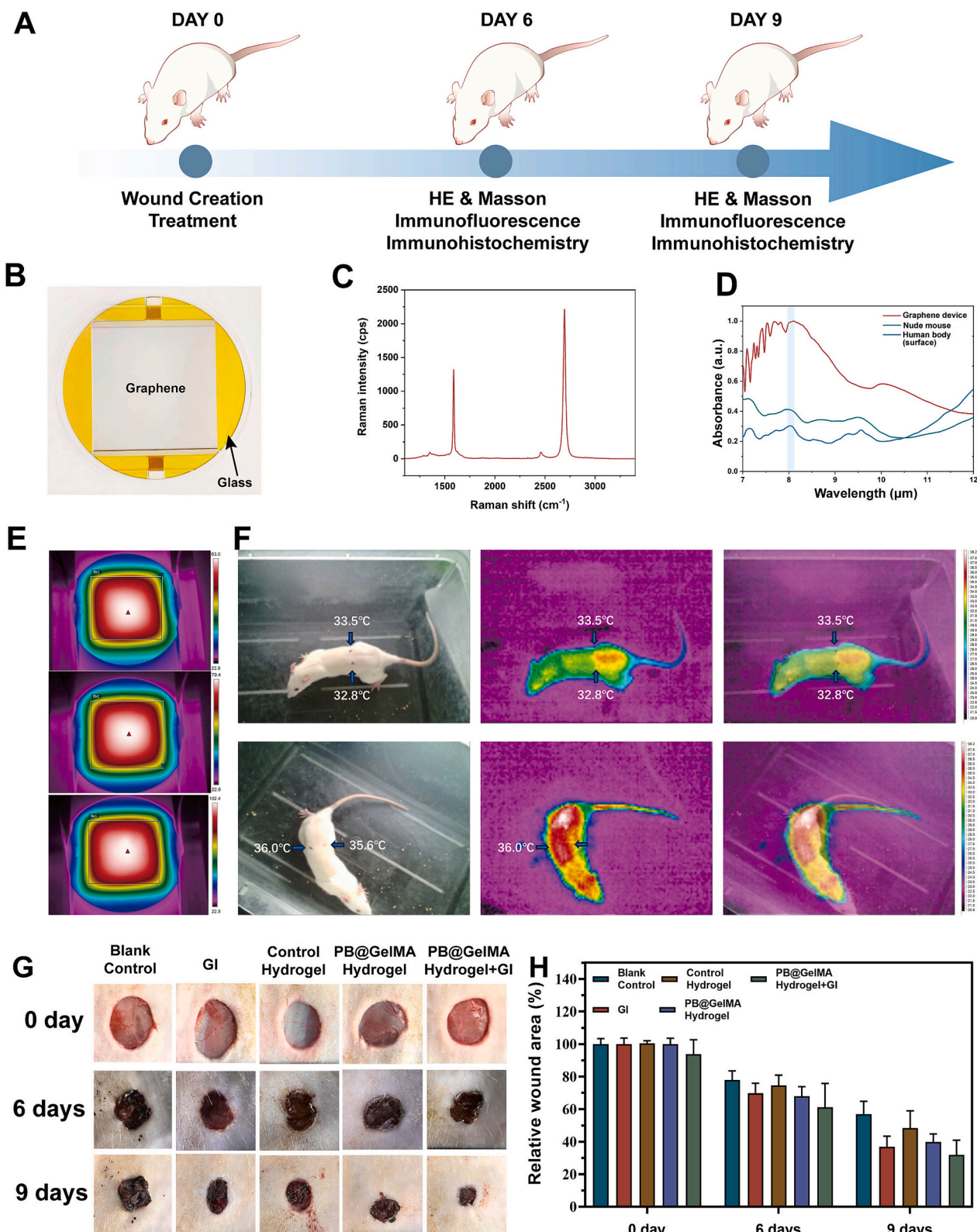


Fig. 5. Synergistic promotion of diabetic wound healing by the special far-infrared radiation generated from the graphene-based device in combination with PB@GelMA nanohybrid hydrogels. A) Schematic diagram of the animal experimental protocol; B) Photograph of the graphene device; C) Raman spectroscopy characterization of the graphene device; D) Comparison of the infrared emission spectra of the graphene device with the absorption spectra of human skin and rat skin (fur removal for experiment), highlighting the blue region; E) Thermographic imaging of the graphene device during heating; F) Optical images before and after infrared irradiation (left), thermographic images (middle), and fused images (right) of the experimental animals; G) Representative photographs of the wounds on days 0, 6, and 9; H) Statistical graph showing the trend of changes in wound area. (For interpretation of the references to colour in this figure legend, the reader is referred to the web version of this article.)

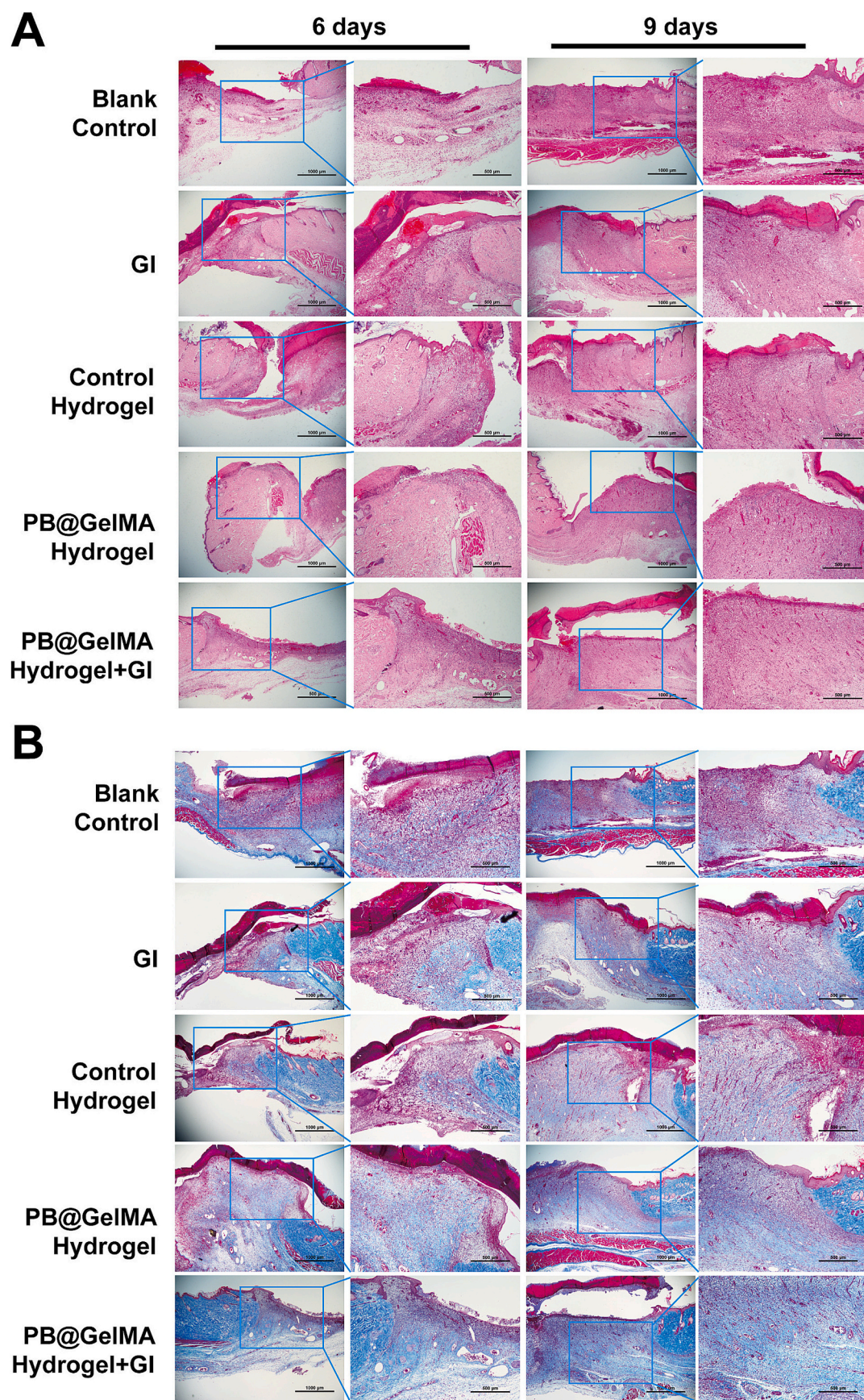


Fig. 6. Histological staining of the wounded tissue: A) Hematoxylin and eosin (H&E) staining; B) Masson's trichrome staining. Scale bars represent: 500 μm (left), 1000 μm (right).

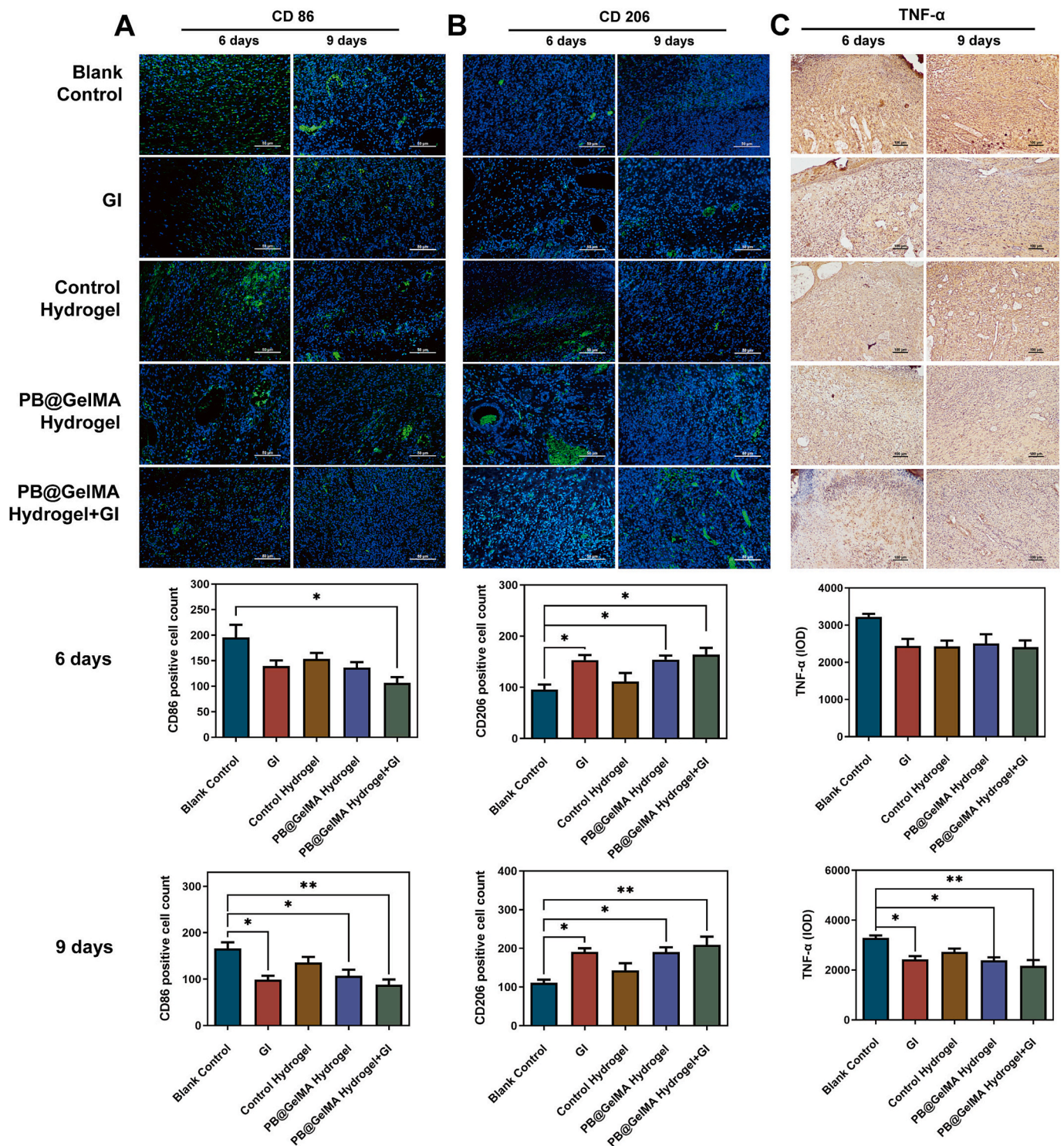


Fig. 7. Immunofluorescence staining of the wounded tissue: A) CD86; B) CD206; C) TNF-α; * $p < 0.05$, ** $p < 0.01$. Scale bars represent: 50 μm (A and B), 100 μm (C).

wound healing (M2-type) macrophage marker CD206 (Fig. 7B) in wound tissues, followed by quantitative analysis of the number of cells positive for these markers. The results showed that, at day 6, both the Prussian blue nanohybrid hydrogel group and the graphene device group exhibited higher levels of CD206 and lower levels of CD86, with these trends being more pronounced in the combined treatment group. Additionally, on day 9, the same trends persisted, with the differences between groups becoming more pronounced. These findings indicate that both the Prussian blue nanohybrid hydrogel and graphene irradiation independently promote a reduction in M1 macrophages and an

increase in M2 macrophages, with their combined application resulting in further enhancement of this effect.

To further confirm the anti-inflammatory effects of the combined use of Prussian blue nanohybrid hydrogel and the graphene device, we evaluated the pro-inflammatory cytokine marker TNF- α using immunohistochemical staining (Fig. 7C). On day 9, TNF- α expression in both the Prussian blue nanohybrid hydrogel group and the combined treatment group with graphene-generated far-infrared radiation was significantly reduced compared to the Blank Control group. Moreover, while both the Prussian blue nanohybrid hydrogel and graphene far-infrared

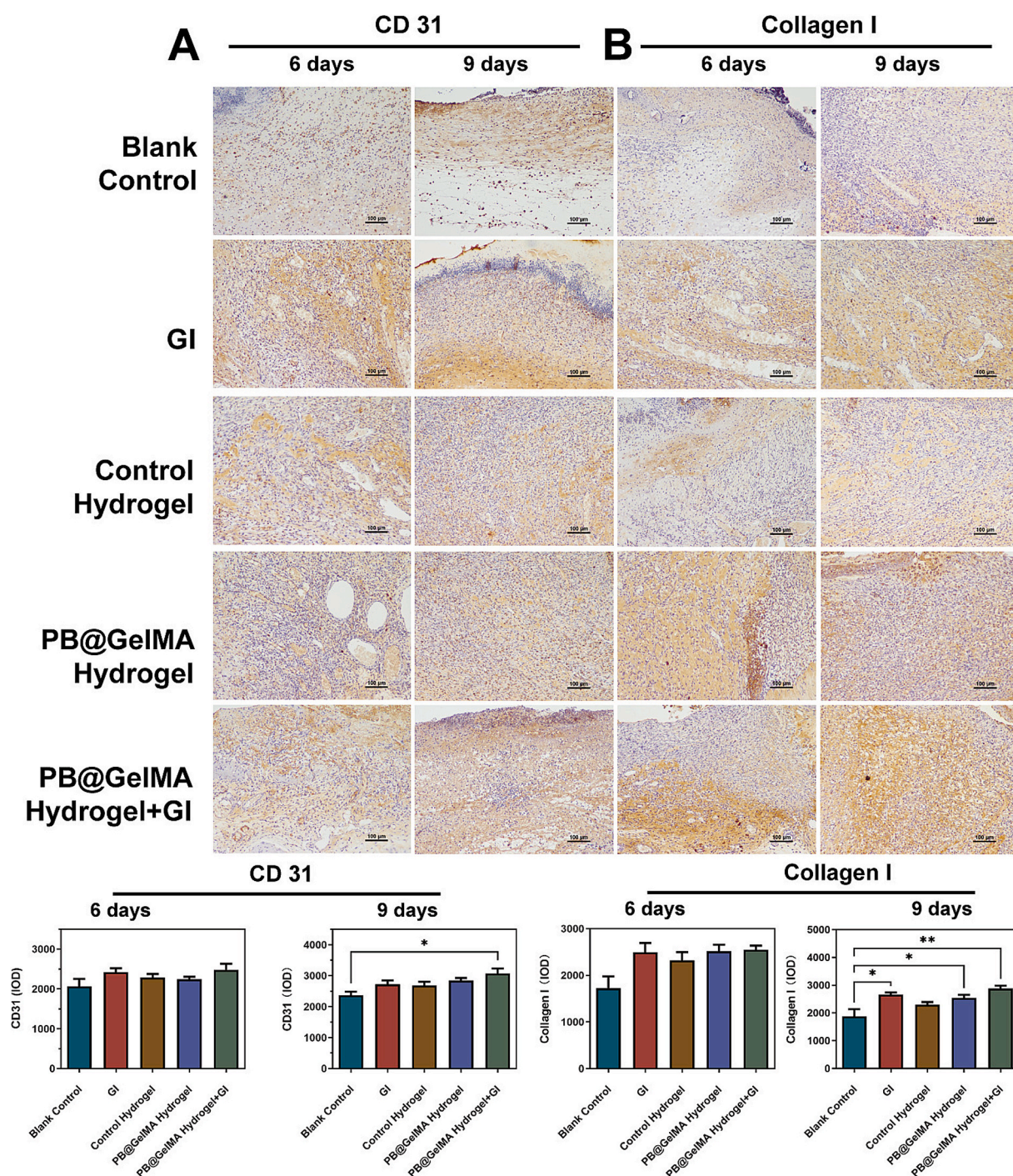


Fig. 8. Immunohistochemical staining characterization of the wounded tissue: A) CD31; B) Type I Collagen. *p < 0.05, **p < 0.01. Scale bars represent 100 μ m.

radiation individually decreased TNF- α expression, the combined treatment demonstrated a significantly stronger effect. These results further validate the ability of the combined therapy to effectively suppress wound inflammation.

To assess neovascularization in the wound tissue, immunohistochemical staining for CD31 was performed (Fig. 8A). On day 9, the combined use of the nanohybrid hydrogel and the graphene device showed higher CD31 expression compared to other groups, which may be attributed to the ability of the nanohybrid hydrogel to ameliorate oxidative stress in the wound microenvironment. These findings suggest that the combination of graphene-generated far-infrared radiation with the nanohybrid hydrogel promotes neovascularization and supports

diabetic wound healing.

Immunohistochemical staining for Collagen I was conducted to evaluate collagen deposition in the granulation tissue (Fig. 8B). Collagen deposition and its aligned orientation play critical roles in the remodeling of the extracellular matrix (ECM). On day 9, the graphene far-infrared treatment group exhibited significantly higher Collagen I levels. This indicates that the combination of graphene-generated far-infrared radiation and the nanohybrid hydrogel facilitates diabetic wound healing by enhancing ECM formation and remodeling.

4. Discussion

In this work, a novel Prussian blue (PB) nanohybrid hydrogel, which differs from previously reported nanohybrid hydrogels in its construction method, was reported. We first conjugated Prussian blue nanoparticles with GelMA to form PB@GelMA nanohybrid units, and subsequently copolymerized these units with other polymer monomers to create the nanohybrid hydrogel. This method enables the hydrogel to better preserve the enzyme-like catalytic activity of the Prussian blue nanoparticles as well as the stability of these particles as crosslinking points within the gel network. Nanozymes, such as those used in this study, possess beneficial properties, including the ability to alleviate wound inflammation or oxidative stress. For example, platinum-based nanozymes particles and dual-network hydrogel dressings developed in our previous studies have demonstrated efficacy in modulating the diabetic wound microenvironment and scavenging oxidative stress in diabetic wounds [35]. However, free nanozymes may pose potential safety risks. To address this, several studies have employed approaches like microneedles to control the release of nanozymes, limiting their entry into the bloodstream and metabolic organs (such as the liver and kidneys), thus improving the safety profile of the materials [43].

In this study, for the first time, we reported a Prussian blue nanohybrid hydrogel by covalently coupling Prussian blue nanoparticles as core sites with methacrylated gelatin (GelMA), forming a new nanohybrid unit. This method covalently fixes the nanoparticles within the hydrogel network, thereby preventing the formation of free-floating nanoparticles and reducing the likelihood of their entry into the bloodstream via wound capillaries, all while maintaining the enzyme-like activity of the Prussian blue. As a result, the safety of the material in the wound healing process is enhanced.

Additionally, we observed a significant temperature dependence of the nanozymes activity within the nanohybrid hydrogel, with enzyme activity being notably higher at 43 °C compared to 37 °C. Therefore, we integrated this nanohybrid hydrogel with a novel graphene-based device developed in our previous work, which emits far-infrared (FIR) radiation to elevate the wound temperature. The combination of the two effectively alleviated inflammation, immune cell infiltration, and promoted wound repair in diabetic wounds. The FIR radiation emitted by the graphene device primarily exhibits a characteristic peak around 8 μm [38,40], which overlaps significantly with the infrared absorption window of human skin tissue. Both this study and previous research have confirmed that FIR radiation in this wavelength range is better absorbed by the body tissues via resonance effects [40]. Moreover, the graphene device used in this study differs considerably from conventional FIR emitters, as it does not follow classical Planck's blackbody radiation law or Wien's displacement law. Notably, the emission wavelength of the device remains stable at approximately 8 μm even with prolonged exposure, without significant blue shift due to changes in device temperature, which ensures higher energy absorption efficiency in the wound. This ability to precisely control the wound temperature enhances the safety of our FIR therapy, and the underlying mechanisms will be further elucidated in the following studies with visualizable *in vitro* systems such as organoids or organoids-on-chip models [44–46].

5. Conclusions

In this study, we developed a novel nanohybrid unit, PB@GelMA, which combines the high cellular affinity and excellent processability of GelMA as a biomimetic material with the nanozymes activity of PB nanoparticles. The resulting PB nanohybrid hydrogels exhibit mechanical properties that closely mimic those of biological tissues, and demonstrate superior reactive oxygen species (ROS) scavenging capability. Furthermore, these hybrid hydrogels can be integrated with non-invasive photothermal therapy based on graphene devices, effectively suppresses inflammation in diabetic rat wounds and promotes wound

healing and tissue regeneration. Taken together, this innovative approach holds considerable promise for advancing the therapeutic potential of diabetic wound healing, and offers new avenues for the development of next generation wound healing treatments.

CRediT authorship contribution statement

Tingting Yu: Writing – review & editing, Writing – original draft, Project administration, Methodology, Investigation, Conceptualization. **Jiamin Zhang:** Writing – review & editing, Writing – original draft, Methodology, Investigation, Data curation. **Junwei Lai:** Methodology, Investigation, Data curation. **Manjiao Deng:** Writing – original draft, Resources, Methodology, Investigation. **Ziying Zhou:** Writing – original draft, Visualization, Investigation. **Zhanbin Xia:** Methodology, Investigation. **Caiping Zhong:** Investigation, Data curation. **Xinyue Feng:** Supervision, Project administration, Formal analysis, Conceptualization. **Yimin Hu:** Writing – original draft, Project administration, Methodology, Investigation, Conceptualization. **XuRan Guo:** Writing – review & editing, Investigation. **Wei Wei:** Writing – review & editing, Investigation. **Weichen Gao:** Writing – review & editing, Investigation. **Yi Zhang:** Writing – review & editing, Writing – original draft, Methodology, Investigation, Data curation. **Zhaobin Guo:** Writing – review & editing, Writing – original draft, Supervision, Resources, Project administration, Funding acquisition, Formal analysis, Data curation, Conceptualization. **Ke Hu:** Writing – review & editing, Writing – original draft, Validation, Supervision, Project administration, Methodology, Investigation, Funding acquisition, Formal analysis, Conceptualization.

Declaration of competing interest

The authors declare that they have no known competing financial interests or personal relationships that could have appeared to influence the work reported in this paper.

Acknowledgments

This work was supported by the National Key Research and Development Program of China (2021YFA1201301), National Science Foundation of China (82304446), Jiangsu Province Capability Improvement Project through Science, Technology and Education (ZDXK202222).

Appendix A. Supplementary data

Supplementary data to this article can be found online at <https://doi.org/10.1016/j.matdes.2025.113839>.

Data availability

Data will be made available on request.

References

- [1] S. Patel, S. Srivastava, M.R. Singh, D. Singh, Mechanistic insight into diabetic wounds: pathogenesis, molecular targets and treatment strategies to pace wound healing, *Biomed. Pharmacother.* 112 (2019) 108615.
- [2] Y. Li, et al., Diabetic vascular diseases: molecular mechanisms and therapeutic strategies, *Signal Transduct. Target. Ther.* 8 (2023) 152.
- [3] Z. Xu, S. Han, Z. Gu, J. Wu, Advances and impact of antioxidant hydrogel in chronic wound healing, *Adv. Healthc. Mater.* 9 (2020) e1901502.
- [4] L. Gao, et al., Intrinsic peroxidase-like activity of ferromagnetic nanoparticles, *Nat. Nanotechnol.* 2 (2007) 577–583.
- [5] W. Zhang, et al., Prussian blue nanoparticles as multienzyme mimetics and reactive oxygen species scavengers, *J. Am. Chem. Soc.* 138 (2016) 5860–5865.
- [6] L. Gao, X. Yan, Nanozymes: biomedical applications of enzymatic Fe(3)O(4) nanoparticles from *in vitro* to *in vivo*, *Adv. Exp. Med. Biol.* 1174 (2019) 291–312.
- [7] M.A. Woo, et al., A novel colorimetric immunoassay utilizing the peroxidase mimicking activity of magnetic nanoparticles, *Int. J. Mol. Sci.* 14 (2013) 9999–10014.

- [8] Z. Tang, H. Wu, Y. Zhang, Z. Li, Y. Lin, Enzyme-mimic activity of ferric nano-core residing in ferritin and its biosensing applications, *Anal. Chem.* 83 (2011) 8611–8616.
- [9] W. Wang, Z. Li, C. Liu, H. Yu, Y. Sun, Application of drug delivery system based on nanozyme cascade technology in chronic wound, *Adv. Healthc. Mater.* 13 (2024) e2402559.
- [10] X. Sun, S. Luo, L. Zhang, Y. Miao, G. Yan, Photodynamic antibacterial activity of oxidase-like nanozyme based on long-lived room-temperature phosphorescent carbon dots, *Food Chem.* 434 (2024) 137541.
- [11] Y. Xu, et al., Microenvironment-responsive metal-phenolic nanozyme release platform with antibacterial, ROS scavenging, and osteogenesis for periodontitis, *ACS Nano* 17 (2023) 18732–18746.
- [12] L. Shang, et al., Ultrasound-augmented multienzyme-like nanozyme hydrogel spray for promoting diabetic wound healing, *ACS Nano* 17 (2023) 15962–15977.
- [13] S. Gao, et al., Multifunctional bioactive nanozyme systems for enhanced diabetic wound healing, *Adv. Healthc. Mater.* (2024) e2401580.
- [14] H. Wang, et al., Nanozyme-enhanced injectable hyaluronic acid-based hydrogel for the treatment of osteoarthritis, *Int. J. Biol. Macromol.* 282 (2024) 136819.
- [15] S. He, et al., A nanoenzyme-modified hydrogel targets macrophage reprogramming-angiogenesis crosstalk to boost diabetic wound repair, *Bioact. Mater.* 35 (2024) 17–30.
- [16] K. Hu, et al., A novel magnetic hydrogel with aligned magnetic colloidal assemblies showing controllable enhancement of magnetothermal effect in the presence of alternating magnetic field, *Adv. Mater.* 27 (2015) 2507–2514.
- [17] H. Xu, et al., Salvaging myocardial infarction with nanoenzyme-loaded hydrogels: targeted scavenging of mitochondrial reactive oxygen species, *J. Control. Release* 375 (2024) 788–801.
- [18] P. Thoniyot, M.J. Tan, A.A. Karim, D.J. Young, X.J. Loh, Nanoparticle-hydrogel composites: concept, design, and applications of these promising, multi-functional materials, *Adv. Sci. (Weinh.)* 2 (2015) 1400010.
- [19] J.Y. Shen, T. Dong, L. Fang, J.J. Ma, L.H. Zeng, Study on multifunctional composite nanomaterials for controlled drug release in biomedicine, *J. Nanosci. Nanotechnol.* 21 (2021) 1230–1235.
- [20] J. Li, et al., Promoting tissue repair using deferoxamine nanoparticles loaded biomimetic gelatin/HA composite hydrogel, *Biomed. Mater.* 19 (2024).
- [21] P. Lavrador, M.R. Esteves, V.M. Gaspar, J.F. Mano, Stimuli-responsive nanocomposite hydrogels for biomedical applications, *Adv. Funct. Mater.* 31 (2021).
- [22] D. Zhang, Y. Chen, M. Hao, Y. Xia, Putting hybrid nanomaterials to work for biomedical applications, *Angew. Chem. Int. Ed. Engl.* 63 (2024) e202319567.
- [23] K. Sahoo, T.R. Gazi, S. Roy, I. Chakraborty, Nanohybrids of atomically precise metal nanoclusters, *Commun. Chem.* 6 (2023) 157.
- [24] G. Guan, M.Y. Han, Functionalized hybridization of 2D nanomaterials, *Adv. Sci. (Weinh.)* 6 (2019) 1901837.
- [25] Y. Wang, et al., Metal nanoparticle hybrid hydrogels: the state-of-the-art of combining hard and soft materials to promote wound healing, *Theranostics* 14 (2024) 1534–1560.
- [26] Q. Li, et al., Enhancing diabetic wound healing with a pH-responsive nanozyme hydrogel featuring multi-enzyme-like activities and oxygen self-supply, *J. Control. Release* 365 (2024) 905–918.
- [27] S. Jiang, et al., Enhanced diabetic wound healing with injectable hydrogel containing self-assembling nanozymes, *J. Control. Release* 372 (2024) 265–280.
- [28] G. Wang, et al., The initiation of oxidative stress and therapeutic strategies in wound healing, *Biomed. Pharmacother.* 157 (2023) 114004.
- [29] Y.-W. Ding, et al., ZnCur nanoparticle-enhanced multifunctional hydrogel platform: synergistic antibacterial and immunoregulatory effects for infected diabetic wound healing, *Chem. Eng. J.* (2024).
- [30] F. Cai, W. Chen, R. Zhao, Y. Liu, Mechanisms of Nrf2 and NF- κ B pathways in diabetic wound and potential treatment strategies, *Mol. Biol. Rep.* 50 (2023) 5355–5367.
- [31] L. He, et al., Photothermal antibacterial materials to promote wound healing, *J. Control. Release* 363 (2023) 180–200.
- [32] T. Paolucci, et al., Electromagnetic field therapy: a rehabilitative perspective in the management of musculoskeletal pain – a systematic review, *J. Pain Res.* 13 (2020) 1385–1400.
- [33] S.B. Rajendran, K. Challen, K.L. Wright, J.G. Hardy, Electrical stimulation to enhance wound healing, *J. Funct. Biomater.* 12 (2021).
- [34] Z. Wang, et al., Intelligent nanozymes: biomimetic design, mechanisms and biomedical applications, *Fundam. Res.* (2024) (in press).
- [35] Z. Zhou, X. Mei, K. Hu, M. Ma, Y. Zhang, Nanohybrid double network hydrogels based on a platinum nanozyme composite for antimicrobial and diabetic wound healing, *ACS Appl. Mater. Interfaces* 15 (2023) 17612–17626.
- [36] K. Hu, et al., Sliced magnetic polyacrylamide hydrogel with cell-adhesive microarray interface: a novel multicellular spheroid culturing platform, *ACS Appl. Mater. Interfaces* 8 (2016) 15113–15119.
- [37] Z. Guo, et al., Fabrication of hydrogel with cell adhesive micropatterns for mimicking the oriented tumor-associated extracellular matrix, *ACS Appl. Mater. Interfaces* 6 (2014) 10963–10968.
- [38] Y. Zhang, et al., Self-organization formation of multicellular spheroids mediated by mechanically tunable hydrogel platform: toward revealing the synergy of chemo- and noninvasive photothermal therapy against colon microtumor, *Macromol. Biosci.* 22 (2022) e2100498.
- [39] Y. Zhang, L. Peng, K. Hu, N. Gu, Stress relaxation-induced colon tumor multicellular spheroid culture based on biomimetic hydrogel for nanoenzyme ferroptosis sensitization evaluation, *Adv. Healthc. Mater.* 12 (2023) e2202009.
- [40] T. Yu, Y. Hu, G. Feng, K. Hu, A graphene-based flexible device as a specific far-infrared emitter for noninvasive tumor therapy, *Adv. Ther.* 3 (2020).
- [41] Z. Li, et al., Engineering mild-photothermal responsive and NO donor Prussian blue nanozymes using mild synthesis for inflammation regulation and bacterial eradication in periodontal disease, *Adv. Mater.* 37 (2025) e2409840.
- [42] D. Lu, et al., DNA-dependent Prussian blue nanoflowers for biosensing, catalysis and imaging, *Adv. Funct. Mater.* 33 (2023) 2208897.
- [43] P. Wang, et al., Enzyme-regulated NO programmed to release from hydrogel-forming microneedles with endogenous/photodynamic synergistic antibacterial for diabetic wound healing, *Int. J. Biol. Macromol.* 226 (2023) 813–822.
- [44] Z. Guo, et al., Visualization of the dynamics of invasion and intravasation of the bacterium that causes Lyme disease in a tissue engineered dermal microvessel model, *Adv. Sci. (Weinh.)* 9 (2022) e2204395.
- [45] Z. Guo, et al., Optical cellular micromotion: a new paradigm to measure tumor cells invasion within gels mimicking the 3D tumor environments, *Small Methods* 6 (2022) e2200471.
- [46] Z. Guo, et al., Validation of a vasculogenesis microfluidic model for radiobiological studies of the human microvasculature, *Adv. Mater. Technol.* 4 (2019) 1800726.